Structural basis for allosteric cross-talk between the asymmetric nucleotide binding sites of a heterodimeric ABC exporter

Michael Hohl[a,b], Lea M. Hürlimann[a,b], Simon Böhm[c], Jendrik Schöppe[a], Markus G. Grütter[a], Enrica Bordignon[c,d], and Markus A. Seeger[a,b,1]

[a]Department of Biochemistry, University of Zurich, CH-8057 Zurich, Switzerland; [b]Institute of Medical Microbiology, University of Zurich, CH-8006 Zurich, Switzerland; [c]Laboratory of Physical Chemistry, Eidgenössische Technische Hochschule Zurich, CH-8093 Zurich, Switzerland; and [d]Freie Universität Berlin, Fachbereich Physik, 14195 Berlin, Germany

ATP binding cassette (ABC) transporters mediate vital transport processes in every living cell. ATP hydrolysis, which fuels transport, displays positive cooperativity in numerous ABC transporters. In particular, heterodimeric ABC exporters exhibit pronounced allosteric coupling between a catalytically impaired degenerate site, where nucleotides bind tightly, and a consensus site, at which ATP is hydrolyzed in every transport cycle. Whereas the functional phenomenon of cooperativity is well described, its structural basis remains poorly understood. Here, we present the apo structure of the heterodimeric ABC exporter TM287/288 and compare it to the previously solved structure with adenosine 5′-(β,γ-imido)triphosphate (AMP-PNP) bound at the degenerate site. In contrast to other ABC exporter structures, the nucleotide binding domains (NBDs) of TM287/288 remain in molecular contact even in the absence of nucleotides, and the arrangement of the transmembrane domains (TMDs) is not influenced by AMP-PNP binding, a notion confirmed by double electron-electron resonance (DEER) measurements. Nucleotide binding at the degenerate site results in structural rearrangements, which are transmitted to the consensus site via two D-loops located at the NBD interface. These loops owe their name from a highly conserved aspartate and are directly connected to the catalytically important Walker B motif. The D-loop at the degenerate site ties the NBDs together even in the absence of nucleotides and substitution of its aspartate by alanine is well-tolerated. By contrast, the D-loop of the consensus site is flexible and the aspartate to alanine mutation and conformational restriction by cross-linking strongly reduces ATP hydrolysis and substrate transport.

membrane transport | X-ray crystallography | allosteric communication

ABC exporters are found in every organism (1, 2). They minimally consist of four domains and exist as homodimers or heterodimers. Two transmembrane domains (TMDs) span the membrane with a total of 12 transmembrane helices and form the substrate permeation pathway by alternating between inward- and outward-oriented states (Fig. S1A). A pair of nucleotide binding domains (NBDs) is connected to the TMDs via coupling helices and drive conformational cycling of the transporter by binding and hydrolysis of ATP, a process which is linked to NBD dimerization and dissociation (3).

In their closed state, the NBDs sandwich two ATP molecules at the dimer interface by composite ATP binding sites involving conserved sequence motifs contributed by both subunits (4, 5). The A-loop and Walker A motif of one NBD and the ABC signature motif of the opposite NBD are involved in nucleotide binding. The Walker B glutamate and the switch-loop histidine constitute a catalytic dyad required for ATP hydrolysis (6, 7). In heterodimeric ABC exporters with asymmetric ATP binding sites, these catalytic residues are noncanonical at the degenerate site and ATP is therefore primarily, if not exclusively, hydrolyzed at the consensus site (8). The Q- and D-loops were associated with

interdomain communication (3, 9–11), but their functional role remains poorly understood.

Recently, we reported the structure of the heterodimeric ABC exporter TM287/288 from the thermophilic bacterium *Thermotoga maritima*, which was crystallized in the presence of adenosine 5′-(β,γ-imido)triphosphate (AMP-PNP) and was shown to transport drugs and dyes when expressed in *Lactococcus lactis* (12). The transporter adopted an inward-facing state with a nucleotide bound exclusively to the degenerate site. In contrast to the inward-oriented structures of MsbA (13), ABCB10 (14), and P-glycoprotein (15–17) in which the NBDs are separated or twisted (18), we found that the NBDs of TM287/288 remain in close contact and do not shift in the NBD dimerization plane (Fig. S1). The current transport mechanism of TM287/288 envisages the binding of a second nucleotide to the consensus site for the transition to the outward-facing NBD-closed state, which subsequently is hydrolyzed to permit resetting of the transporter (12).

Here, we present the high-resolution structure of the nucleotide-free state of TM287/288. Despite high ATP concentrations in the cell, this state is transiently adopted during transport; at the

Significance

ATP binding cassette (ABC) exporters contain a pair of nucleotide-binding domains (NBDs), which bind and hydrolyze ATP to pump substrates across the membrane. Functional studies suggest that the two ATP binding sites are conformationally coupled. In contrast to other ABC exporters, we show that the asymmetric NBDs of the heterodimeric ABC exporter TM287/288 remain in contact, even in the absence of nucleotides. By comparing the apo state with the adenosine 5′-(β,γ-imido)triphosphate–bound structure of TM287/288, we unravel the structural basis for allosteric coupling between the ATP binding sites. NBD-NBD contacts in the inward-facing transporter warrant cross-communication between the ATP binding sites throughout the transport cycle and are in agreement with functional models of clinically important heterodimeric ABC exporters including CFTR, SUR1, and TAP1/2.

BIOCHEMISTRY

consensus site, the hydrolysis product ADP is replaced by ATP in each transport cycle, and at the degenerate site, the bound nucleotide is occasionally exchanged. We show that the asymmetric NBDs of TM287/288 remain in contact even in the absence of nucleotides. By comparing the apo state with the AMP-PNP–bound structure, we unravel the structural basis for allosteric coupling between the ATP binding sites.

Results

In the Absence of Nucleotides, the NBDs of TM287/288 Remain in Contact. To gain insight into the functional and structural role of nucleotide binding at the degenerate site, we solved the crystal structure of TM287/288 in its apo state at 2.53 Å resolution (Table S1). Space group and cell edges of the apo state crystals were identical to the ones obtained in the presence of AMP-PNP and, therefore, structural changes discussed here are independent from crystal packing. The overall structures of the apo and the nucleotide-bound state of TM287/288 are highly similar [rmsd of 0.636 Å over residues 1–569 (chain A) and 10–592 (chain B)] and show that the NBDs remain in contact even in the absence of nucleotides (Fig. 1 A and B).

To examine conformational changes as a result of nucleotide binding in solution, four spin-label pairs were introduced into TM287/288: one in the extracellular region ($150^{TM287}/295^{TM288}$), one in the intracellular region ($131^{TM288}/248^{TM288}$) of the TMDs, and two in the asymmetric NBDs ($350^{TM287}/475^{TM288}$ and $460^{TM287}/363^{TM288}$) (Fig. 1B). For the double electron-electron resonance (DEER) measurements, the spin-labeled transporters were incubated at room temperature in the presence or absence

of AMP-PNP and $MgCl_2$ before flash freezing in cold liquid pentane (Fig. 1 C–F and Fig. S2).

The experimental DEER distances agree with those simulated with a rotamer library approach (19) on the two available crystal structures, considering the 3 to 3.5 Å accuracy achievable with this method (20) (Fig. 1 C–F and Table S2). The DEER measurements with the spin-label pairs $350^{TM287}/475^{TM288}$ and $460^{TM287}/363^{TM288}$ strongly support the crystal structures in which the NBDs of TM287/288 remain connected in the absence of nucleotides, because the frozen conformational ensembles in the apo and AMP-PNP–bound states are almost indistinguishable.

The Conformational Equilibrium of TM287/288 Is Shifted Toward the Inward-Facing State in the Presence of AMP-PNP. In agreement with the crystal structures, but in contrast to what was observed for the homodimeric ABC exporter MsbA (21, 22), we found that all intracellular and extracellular interspin distances were only slightly influenced by AMP-PNP addition. We noted a small distance decrease in the intracellular pairs $131^{TM288}/248^{TM288}$ and $350^{TM287}/475^{TM288}$ upon AMP-PNP binding as well as a slight distance increase in the NBD pair $460^{TM287}/363^{TM288}$ (Fig. 1 D–F and Table S2), indicative of AMP-PNP binding and consequent allosteric effects in the intracellular region of the exporter. There are two reasons that let us interpret these changes resulting from side-chain rearrangements at the spin-labeled sites and not from the switch to the outward-facing conformation of the exporter. First, the transition to the outward-facing state modeled using Sav1866 (3) as a template is expected to induce a more pronounced interspin distance decrease in all
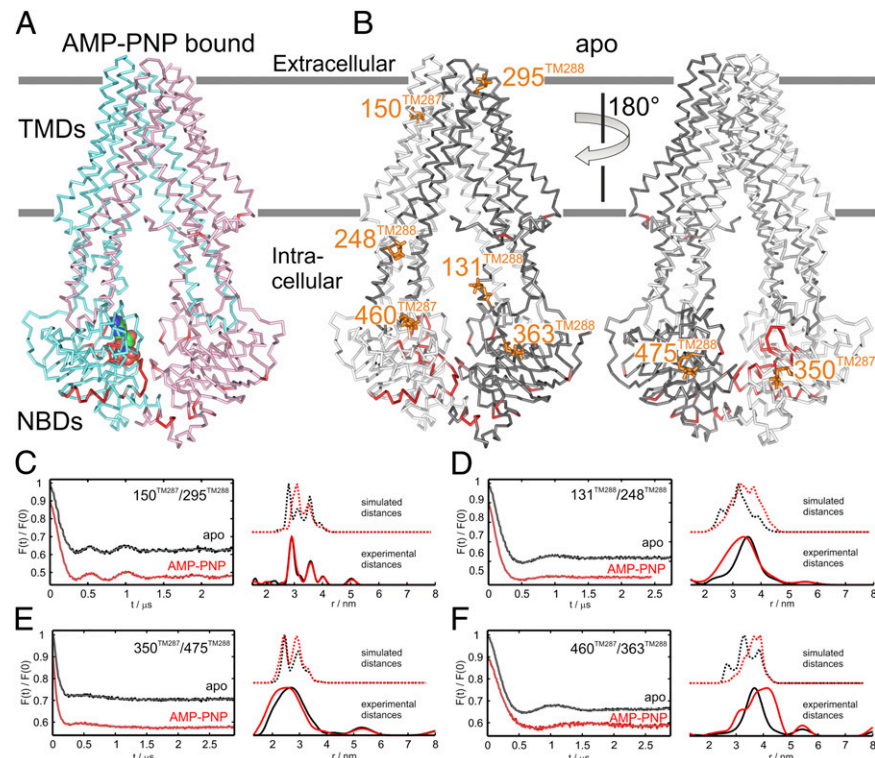

Fig. 1. Structural differences between the apo and the nucleotide-bound TM287/288 structures. (A) Side view of the nucleotide-bound TM287/288 structure colored in cyan (TM287) and pink (TM288). AMP-PNP is depicted as colored spheres. C_α positions deviating by more than 1.1 Å between the nucleotide-bound and the apo structure are highlighted in red. Membrane boundaries are indicated in gray. (B) The structural differences are highlighted on the apo structure. TM287 is shown in light gray and TM288 in dark gray. Spin labels used for DEER analysis are shown as orange sticks. (C–F) DEER measurements of four spin-label pairs: in the extracellular region ($150^{TM287}/295^{TM288}$) (C), in the intracellular region of the TMDs ($131^{TM288}/248^{TM288}$) (D), in the NBDs at the degenerate site ($350^{TM287}/475^{TM288}$) (E), and in the NBDs at the consensus site ($460^{TM287}/363^{TM288}$) (F). Left graphs show background-corrected DEER traces [F(t)/F(0)] in the absence of nucleotides (black) and in the presence of AMP-PNP and $MgCl_2$ (red). Right graphs show experimental distance distributions (solid lines at the bottom) and simulated distances based on the two corresponding X-ray structures (dotted lines above).

three pairs (>1 nm) and a concomitant distance increase in the extracellular pair. Second, similar small variations in the mean distances are simulated on the two corresponding structures, corroborating the notion that they can be explained by side-chain rearrangements alone (Fig. 1 C–F and Table S2).

To address possible influence of the detergent on the conformational cycling of TM287/288, the exporter spin-labeled at the intracellular pair $131^{TM288}/248^{TM288}$ was reconstituted in liposomes. The experimental mean distances in liposomes were similar to those obtained in detergent with deviations in the mean distances of 2.0 and 3.6 Å, in the apo and AMP-PNP–bound state, respectively (Fig. S3 A and B and Table S2).

The DEER measurements seemingly contradict cross-linking experiments showing that AMP-PNP facilitates NBD closure in TM287/288 (12). However, cross-links irreversibly trap states even if they are only marginally populated. The DEER measurements suggest that in solution, the conformational equilibrium is strongly shifted toward the inward-facing state, because the population representing the outward-facing state was not detectable.

Structural Consequences of Nucleotide Binding at the Degenerate Site. The majority of structural differences between the apo and the nucleotide-bound state are located at NBD1 (TM287) (Fig. 2 and Movie S1). Residues directly contacting AMP-PNP in the nucleotide-bound structure including the A-loop, the Walker A motif, and the helix following Walker A respond strongly to nucleotide binding (Fig. 2C and Fig. S4). The hydrogen bonding network connecting the NBDs at the degenerate site, involving $Asn521^{TM288}$ of the D-loop, $Thr368^{TM287}$ of the Walker A motif, and $Gln526^{TM287}$ of the switch-loop is rearranged. The number of inter-NBD hydrogen bonds is reduced from seven in the AMP-

PNP–bound structure to four in the apo state (Fig. 3 A and B). Despite the rearrangements, the distance between the NBDs remains unchanged. In the apo state, a hydrogen bond between the ABC signature motif serine ($Ser493^{TM288}$) and the D-loop aspartate ($Asp523^{TM288}$) of NBD2 (TM288) is formed, and conformational differences are also observed in residues following the Q-loop of NBD2 (Fig. 3B and Fig. S4F). These residues directly interact with the coupling helix of TM287 and, thereby, would allow for conformational communication between the degenerate site and the TMDs. However, we did not observe structural changes at the coupling helix. When $Asp523^{TM288}$ was mutated to alanine, the ATPase activity of TM287/288 increased approximately twofold, suggesting that the $Ser493^{TM288}$–$Asp523^{TM288}$ interaction slows down the catalytic cycle (Fig. 3C and Fig. S5). However, other contacts made by the $Asp523^{TM288}$ side chain during the catalytic cycle may also play a role. In addition, the apparent affinity of ATP hydrolysis was decreased from 20.3 ± 1.3 μM to 71.8 ± 4.0 μM (SEM derived from nonlinear regression analysis). $Asp523^{TM288}$ is preceded by $Glu517^{TM288}$ of the Walker B motif, which is essential for ATP hydrolysis at the consensus site (Fig. 4B), suggesting that the D-loop of NBD2 allosterically couples the degenerate and the consensus site.

Conformational Coupling Mediated by a Flexible Consensus Site D-Loop. The biggest structural differences are observed at the D-loop of NBD1, which is part of the consensus site (Fig. 2C). When AMP-PNP binds to the degenerate site, the D-loop aspartate ($Asp501^{TM287}$) forms two hydrogen bonds with the Walker A motif of NBD2 (Fig. 3A). These hydrogen bonds are broken in the apo state, and the D-loop and the associated D-loop helix undergo major conformational rearrangements
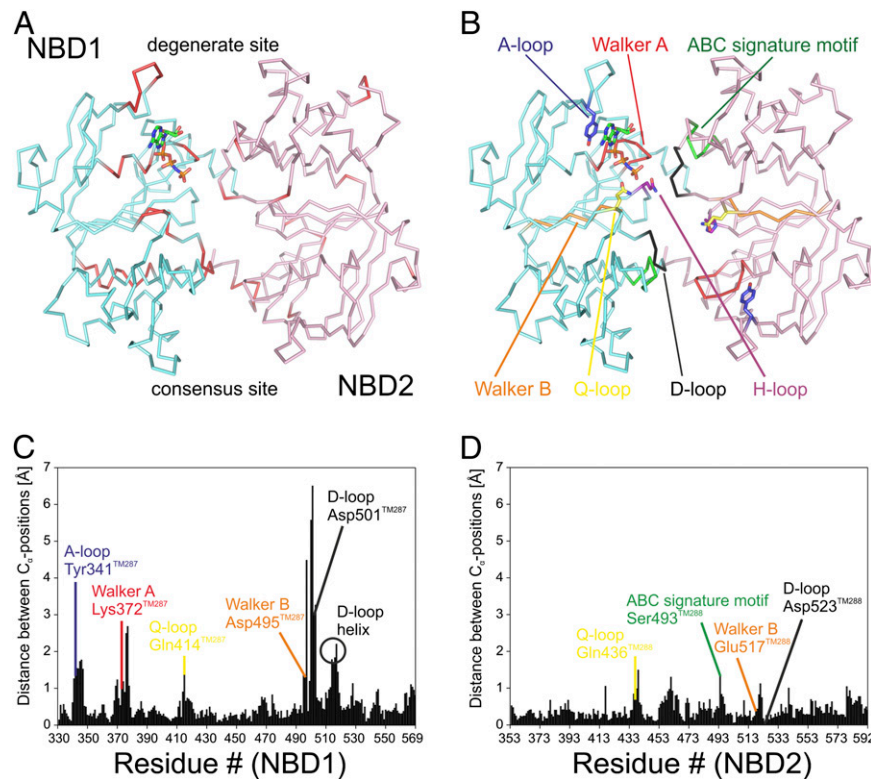

Fig. 2. Conformational changes within the NBDs in response to nucleotide binding. (A) Top view on the NBD dimer (NBD1, Gly330-Phe569; NBD2, Gly353-Leu593) with bound AMP-PNP and structural changes accentuated as in Fig. 1. (B) NBD dimer with conserved motifs highlighted in colors. (C and D) The absolute backbone carbon distances between each residue of the nucleotide-bound and the apo state of NBD1 (C) and NBD2 (D) are plotted against the residue number. Key residues of conserved NBD motifs are labeled.
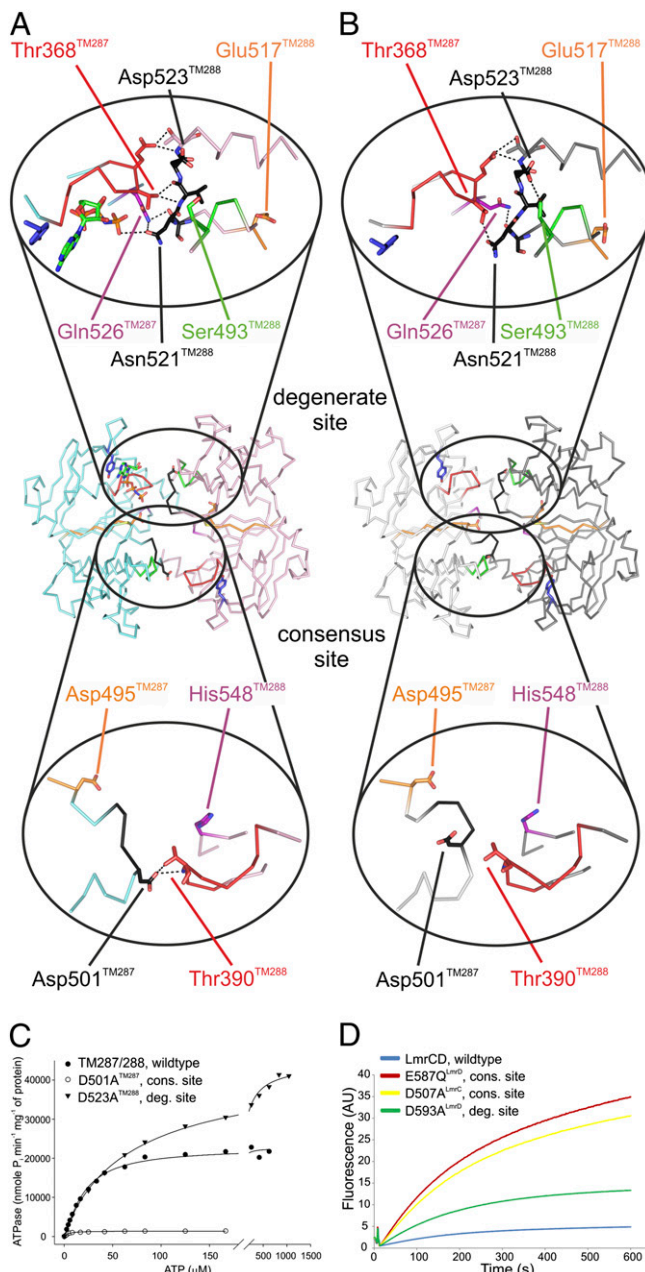
Fig. 3. NBD–NBD interactions mediated by the D-loops. (*A* and *B*) Hydrogen-bonding networks (≤3.6 Å) at the degenerate (*Upper*) and the consensus site (*Lower*) of the AMP-PNP–bound (*A*) and the apo (*B*) structure are depicted. (*C*) ATPase activities of D-loop mutants D501A^{TM287} and D523A^{TM288} introduced at the consensus and the degenerate site of TM287/288 were determined at varying ATP concentrations. The scale between 0 and 200 μM ATP is expanded. (*D*) Transport of BCECF-AM mediated by the D-loop mutants D507A^{LmrC} and D593A^{LmrD} was measured in *L. lactis* ΔlmrA ΔlmrCD. The inactive E587Q^{LmrD} mutant served as negative control.

(Fig. 3 *A* and *B*). In the apo structure, the temperature factors of the D-loop residues are elevated, suggesting conformational flexibility (Fig. S6). To investigate the functional importance of the Asp501^{TM287}-mediated hydrogen bonds, this highly conserved residue was mutated to alanine. The mutation caused a 16-fold decrease of the maximal ATPase activity and a fivefold increase of the apparent ATP affinity (Fig. 3*C* and Fig. S5).

Each D-loop mutation was combined with the intracellular spin label pair 131^{TM288}/248^{TM288} for DEER analysis. The distances in

the apo and AMP-PNP–bound states were found to be similar to those obtained in the wild-type background (Fig. S3 *C* and *D* and Table S2). However, the reproducible distance decrease observed in the original 131^{TM288}/248^{TM288} pair upon AMP-PNP binding could not be detected in any of the D-loop mutants, indicating allosteric interference in the rearrangement of the side chains in the intracellular region of the transporter.

Both D-loop mutations were additionally introduced into LmrCD (D507A in LmrC and D593A in LmrD), a well-characterized TM287/288 homolog from *L. lactis* sharing a sequence identity of 36% (23, 24). When expressing the D507A^{LmrC} consensus site mutant in *L. lactis* ΔlmrA ΔlmrCD, transport of the dyes Hoechst 33342 and BCECF-AM was found to be severely affected (Fig. 3*D* and Fig. S7). In contrast, the D593A^{LmrD} mutation introduced at the degenerate site only mildly affected LmrCD-mediated transport, confirming the asymmetric nature of the D-loops in heterodimeric ABC exporters.

Restriction of the Flexible Consensus Site D-Loop Inhibits ATP Hydrolysis.

The D-loop of NBD1 is preceded by the Walker B motif harboring the Walker B aspartate (Asp494^{TM287}). In the AMP-PNP–bound structure, but not in the apo state, Asp494^{TM287} establishes a hydrogen bond to Ser373^{TM287} of the Walker A motif, that, in turn, coordinates the catalytically essential magnesium ion (Fig. 4*A* and Fig. S4*D*). In this manner, the Walker B motif senses the presence of the nucleotide–magnesium complex at the degenerate site and transmits this information in a long-range interaction via the D-loop to the Walker A motif of the consensus site. To further support this structural observation, we engineered a disulfide cross-link between the two D-loops by mutating Ser498^{TM287} and Ser520^{TM288} into cysteines in a cysteine-free background. Despite distances of 7.7 Å and 10.1 Å between the thiol groups in the nucleotide-bound and the apo state, respectively, a cross-link between these two cysteines was spontaneously formed during protein purification (Fig. 4*C*). Crystals of the cross-linked mutant diffracted to 3.2 Å, and the resulting structure confirmed the expected tethering of the flexible NBD1 D-loop to the comparatively solid NBD2 D-loop, whose structure remains largely unchanged (Fig. 4*D*). Although AMP-PNP was added for crystallization of the cross-linked mutant, no additional electron density at the degenerate site was observed. The ATPase activity of the cross-linked mutant was reduced to 15% of cysteine-free TM287/288 and was fully restored by the addition of DTT (Fig. 4*C*). Hence, D-loop flexibility in NBD1 is a requirement for nucleotide binding at the degenerate site and for ATP hydrolysis at the consensus site.

Discussion

The involvement of the D-loop in NBD-NBD interdomain communication has first been postulated based on structures of isolated, homodimeric NBDs (5, 9). However, there are only a few reports that describe its functional role. A systematic cysteine-scanning study of residues lining the NBD interface of the sulfonylurea receptor SUR1 highlighted D-loop residues to play a key role in MgADP stimulation of its associated potassium channel subunit (25). Of special note, substituting the degenerate site D-loop aspartate by a cysteine (D1513C) completely abolished MgADP stimulated potassium channel gating, whereas the functional impact of the corresponding consensus site mutant (D861C) was less severe. Although these results stand in contrast to the transport assays performed with LmrCD in which the consensus site D-loop mutant was most severely affected, they highlight the functional importance of the D-loops in heterodimeric ABC exporters. Mutations in the D-loop (L511P and D512G) of the homodimeric lipid A transporter MsbA, which abolish the function of this essential transporter in *Escherichia*
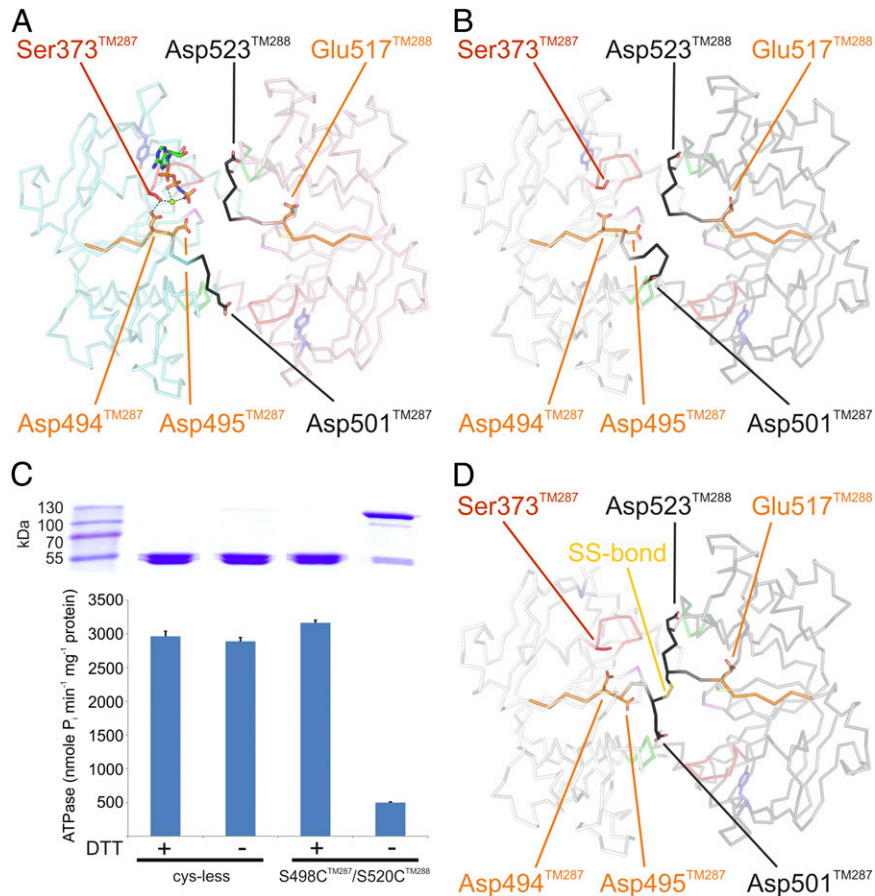
Fig. 4. Long-range interactions connecting the degenerate with the consensus site. (*A* and *B*) Walker B motifs (orange) and the D-loops (black) are highlighted in the AMP-PNP–bound (*A*) and the apo (*B*) structure. Residues critical for cross-communication between the two ATP binding sites are highlighted. AMP-PNP is shown as sticks and Mg^{2+} as green sphere. (*C*) Functional analysis of the cross-linked S498C^{TM287}/S520C^{TM288} mutant by SDS/PAGE (*Upper*) and corresponding ATPase activities (*Lower*). Cys-less TM287/288 served as control. DTT was added where indicated. (*D*) Crystal structure of the cross-linked S498C^{TM287}/S520C^{TM288} mutant. The disulfide bond is depicted as sticks.

coli were initially discovered by random mutagenesis (26). Biochemical analysis of these mutants revealed that the L511P mutant is defective in ATP hydrolysis, which could explain its lacking transport function (27). The D512G mutant, however, exhibited a threefold increased ATPase activity, reminiscent to the D523A^{TM288} mutation introduced at the degenerate site D-loop of TM287/288. The inability of the D512G mutant to transport lipid A was explained with a coupling defect to the transmembrane domains. In light of the structural observations presented in this study, we speculate that cross-talk between the two ATP binding sites of MsbA is likely to be disturbed in the D512G mutant and might explain the observed loss of transport function.

Comparison of the apo and the AMP-PNP–bound structures of TM287/288 allow for the first time, to our knowledge, an analysis of allosteric cross-talk between ATP binding sites in the context of a full-length ABC exporter. We provide structural and functional evidence that both D-loops of TM287/288 and LmrCD play a role in allosteric coupling, although in an asymmetric manner. The D-loop of NBD2 is integral part of the degenerate ATP binding site and, thereby, ties the NBDs together even in the absence of nucleotides. By contrast, the D-loop of NBD1 is highly flexible and contacts NBD2 via its conserved aspartate side chain only if the degenerate site is occupied with a nucleotide. Importantly, the consensus site D-loop aspartate was found to be critical for ATP hydrolysis in TM287/288 and substrate transport in LmrCD.

In contrast to other inward-oriented ABC exporters in which the NBDs are separated or twisted (Fig. S1), the arrangement of the NBDs as seen in TM287/288 allows for allosteric communication between the two ATP binding sites during the entire transport cycle. Our structural observations are likely to be of functional relevance to understand well-studied heterodimeric ABC exporters of eukaryotic origin. For example, the generally accepted mechanistic model of CFTR envisages the degenerate site to be constantly closed during the entire gating cycle, a notion supported by the fact that nucleotides bind more tightly to the degenerate than to the consensus site of CFTR (28). Despite some disputes whether the degenerate site changes its conformation as the channel progresses through its states (29, 30), there is unanimous agreement that inter-NBD contacts need to be established at all times to explain the experimentally observed cross-talk between the degenerate and the consensus site. As suggested recently (30), a partially opened degenerate site as seen in TM287/288 does not contradict current functional models of CFTR, but rather could explain how the ATP binding sites sustain their ability to cross-communicate while the TMDs adopt an inward-facing closed-channel state.

In contrast to the well-studied homodimeric ABC transporter MsbA (21, 22), AMP-PNP did not lead to NBD closure and the transition to the outward-facing state in TM287/288, suggesting that major differences exist between the two ABC exporters in the response to this nucleotide analog. Studies on CFTR and SUR1 revealed that AMP-PNP is a poor ATP analog in heterodimeric

ABC exporters. For CFTR, a 20-fold decreased opening rate was observed for AMP-PNP compared with ATP (31) and in SUR1, AMP-PNP fails to support NBD dimerization and conformational switching (32).

In conclusion, our analysis provides unprecedented mechanistic insight into the cross-communication between asymmetric nucleotide binding sites of heterodimeric ABC exporters and underscores the importance of nucleotide binding at the degenerate site to modulate the catalytic activity of the consensus site and, thus, substrate transport. The presented work offers a structural rationale for future studies on mammalian ABC exporters with asymmetric ATP-binding sites including the medically important transporters MRP1, SUR1, TAP1/2, and CFTR (33–36).

Methods

TM287/288 was purified as described (12) and yielded apo state crystals, which diffracted anisotropically to 2.53 Å. For DEER measurements in detergent solution, double cys-mutants of TM287/288 were spin-labeled with MTSL [(1-oxyl-2,2,5,5-tetramethyl-Δ3-pyrroline-3-methyl) methanethiosulfonate] and incubated in the presence or absence of 2.5 mM AMP-PNP and 2.5 mM MgCl$_2$ at 25 °C prior to flash freezing in cold liquid pentane. DEER traces were recorded at Q band with all pulses set to 12 ns and frequency separation of 100 MHz (37). Data analysis and simulation of the MTSL rotamers on the X-ray structures were performed with the softwares DeerAnalysis2013 (38) and MMM2013.2 (19). The D-loop aspartates of TM287/288 and LmrCD were substituted by alanines using site-directed mutagenesis. ATPase activities of TM287/288 mutants were measured by determining liberated phosphate. Transport of the fluorescent dyes Hoechst 33342 and BCECF-AM by LmrCD was measured in *Lactococcus lactis*. Experimental details are described in *SI Methods*.

1. Seeger MA, van Veen HW (2009) Molecular basis of multidrug transport by ABC transporters. *Biochim Biophys Acta* 1794(5):725–737.
2. Davidson AL, Dassa E, Orelle C, Chen J (2008) Structure, function, and evolution of bacterial ATP-binding cassette systems. *Microbiol Mol Biol Rev* 72(2):317–364.
3. Dawson RJ, Locher KP (2006) Structure of a bacterial multidrug ABC transporter. *Nature* 443(7108):180–185.
4. Hopfner KP, et al. (2000) Structural biology of Rad50 ATPase: ATP-driven conformational control in DNA double-strand break repair and the ABC-ATPase superfamily. *Cell* 101(7):789–800.
5. Smith PC, et al. (2002) ATP binding to the motor domain from an ABC transporter drives formation of a nucleotide sandwich dimer. *Mol Cell* 10(1):139–149.
6. Orelle C, Dalmas O, Gros P, Di Pietro A, Jault JM (2003) The conserved glutamate residue adjacent to the Walker-B motif is the catalytic base for ATP hydrolysis in the ATP-binding cassette transporter BmrA. *J Biol Chem* 278(47):47002–47008.
7. Oldham ML, Chen J (2011) Snapshots of the maltose transporter during ATP hydrolysis. *Proc Natl Acad Sci USA* 108(37):15152–15156.
8. Procko E, O'Mara ML, Bennett WF, Tieleman DP, Gaudet R (2009) The mechanism of ABC transporters: General lessons from structural and functional studies of an antigenic peptide transporter. *FASEB J* 23(5):1287–1302.
9. Zaitseva J, et al. (2006) A structural analysis of asymmetry required for catalytic activity of an ABC-ATPase domain dimer. *EMBO J* 25(14):3432–3443.
10. Urbatsch IL, Gimi K, Wilke-Mounts S, Senior AE (2000) Investigation of the role of glutamine-471 and glutamine-1114 in the two catalytic sites of P-glycoprotein. *Biochemistry* 39(39):11921–11927.
11. Jones PM, George AM (2012) Role of the D-loops in allosteric control of ATP hydrolysis in an ABC transporter. *J Phys Chem A* 116(11):3004–3013.
12. Hohl M, Briand C, Grütter MG, Seeger MA (2012) Crystal structure of a heterodimeric ABC transporter in its inward-facing conformation. *Nat Struct Mol Biol* 19(4):395–402.
13. Ward A, Reyes CL, Yu J, Roth CB, Chang G (2007) Flexibility in the ABC transporter MsbA: Alternating access with a twist. *Proc Natl Acad Sci USA* 104(48):19005–19010.
14. Shintre CA, et al. (2013) Structures of ABCB10, a human ATP-binding cassette transporter in apo- and nucleotide-bound states. *Proc Natl Acad Sci USA* 110(24):9710–9715.
15. Aller SG, et al. (2009) Structure of P-glycoprotein reveals a molecular basis for polyspecific drug binding. *Science* 323(5922):1718–1722.
16. Jin MS, Oldham ML, Zhang Q, Chen J (2012) Crystal structure of the multidrug transporter P-glycoprotein from Caenorhabditis elegans. *Nature* 490(7421):566–569.
17. Li J, Jaimes KF, Aller SG (2014) Refined structures of mouse P-glycoprotein. *Protein Sci* 23(1):34–46.
18. Moradi M, Tajkhorshid E (2013) Mechanistic picture for conformational transition of a membrane transporter at atomic resolution. *Proc Natl Acad Sci USA* 110(47):18916–18921.
19. Polyhach Y, Bordignon E, Jeschke G (2011) Rotamer libraries of spin labelled cysteines for protein studies. *Phys Chem Chem Phys* 13(6):2356–2366.
20. Jeschke G (2013) Conformational dynamics and distribution of nitroxide spin labels. *Prog Nucl Magn Reson Spectrosc* 72:42–60.
21. Zou P, Bortolus M, McHaourab HS (2009) Conformational cycle of the ABC transporter MsbA in liposomes: Detailed analysis using double electron-electron resonance spectroscopy. *J Mol Biol* 393(3):586–597.
22. Mittal A, Böhm S, Grütter MG, Bordignon E, Seeger MA (2012) Asymmetry in the homodimeric ABC transporter MsbA recognized by a DARPin. *J Biol Chem* 287(24):20395–20406.
23. Lubelski J, et al. (2006) LmrCD is a major multidrug resistance transporter in Lactococcus lactis. *Mol Microbiol* 61(3):771–781.
24. Seeger MA, et al. (2012) Tuning the drug efflux activity of an ABC transporter *in vivo* by in vitro selected DARPin binders. *PLoS ONE* 7(6):e37845.
25. Masia R, Nichols CG (2008) Functional clustering of mutations in the dimer interface of the nucleotide binding folds of the sulfonylurea receptor. *J Biol Chem* 283(44):30322–30329.
26. Polissi A, Georgopoulos C (1996) Mutational analysis and properties of the msbA gene of Escherichia coli, coding for an essential ABC family transporter. *Mol Microbiol* 20(6):1221–1233.
27. Schultz KM, Merten JA, Klug CS (2011) Effects of the L511P and D512G mutations on the Escherichia coli ABC transporter MsbA. *Biochemistry* 50(13):2594–2602.
28. Basso C, Vergani P, Nairn AC, Gadsby DC (2003) Prolonged nonhydrolytic interaction of nucleotide with CFTR's NH2-terminal nucleotide binding domain and its role in channel gating. *J Gen Physiol* 122(3):333–348.
29. Tsai MF, Li M, Hwang TC (2010) Stable ATP binding mediated by a partial NBD dimer of the CFTR chloride channel. *J Gen Physiol* 135(5):399–414.
30. Csanády L, Mihályi C, Szollosi A, Töröcsik B, Vergani P (2013) Conformational changes in the catalytically inactive nucleotide-binding site of CFTR. *J Gen Physiol* 142(1):61–73.
31. Vergani P, Nairn AC, Gadsby DC (2003) On the mechanism of MgATP-dependent gating of CFTR Cl- channels. *J Gen Physiol* 121(1):17–36.
32. Ortiz D, Gossack L, Quast U, Bryan J (2013) Reinterpreting the action of ATP analogs on K(ATP) channels. *J Biol Chem* 288(26):18894–18902.
33. Weekes MP, et al. (2013) Latency-associated degradation of the MRP1 drug transporter during latent human cytomegalovirus infection. *Science* 340(6129):199–202.
34. Aittoniemi J, et al. (2009) Review. SUR1: A unique ATP-binding cassette protein that functions as an ion channel regulator. *Philos Trans R Soc Lond B Biol Sci* 364(1514):257–267.
35. Herget M, et al. (2011) Conformation of peptides bound to the transporter associated with antigen processing (TAP). *Proc Natl Acad Sci USA* 108(4):1349–1354.
36. Gadsby DC, Vergani P, Csanády L (2006) The ABC protein turned chloride channel whose failure causes cystic fibrosis. *Nature* 440(7083):477–483.
37. Polyhach Y, et al. (2012) High sensitivity and versatility of the DEER experiment on nitroxide radical pairs at Q-band frequencies. *Phys Chem Chem Phys* 14(30):10762–10773.
38. Jeschke G, et al. (2006) DeerAnalysis2006 - a comprehensive software package for analyzing pulsed ELDOR data. *Appl Magn Reson* 30(3-4):473–498.